


# The phase diagrams of $\text{KCaF}_3$ and $\text{NaMgF}_3$ by ab initio simulations

Clément Jakymiw<sup>1</sup> · Lidunka Vočadlo<sup>2</sup> · David P. Dobson<sup>2</sup> · Edward Bailey<sup>2</sup> · Andrew R. Thomson<sup>2</sup> · John P. Brodholt<sup>2</sup> · Ian G. Wood<sup>2</sup>  · Alex Lindsay-Scott<sup>2</sup>

Received: 6 May 2015 / Accepted: 1 September 2017  
© The Author(s) 2017. This article is an open access publication

**Abstract**  $\text{ABF}_3$  compounds have been found to make valuable low-pressure analogues for high-pressure silicate phases that are present in the Earth's deep interior and that may also occur in the interiors of exoplanets. The phase diagrams of two of these materials,  $\text{KCaF}_3$  and  $\text{NaMgF}_3$ , have been investigated in detail by static ab initio computer simulations based on density functional theory. Six  $\text{ABF}_3$  polymorphs were considered, as follows: the orthorhombic perovskite structure ( $\text{GdFeO}_3$ -type; space group  $Pbnm$ ); the orthorhombic  $\text{CaIrO}_3$  structure ( $Cmcm$ ; commonly referred to as the “post-perovskite” structure); the orthorhombic  $\text{Sb}_2\text{S}_3$  and  $\text{La}_2\text{S}_3$  structures (both  $Pmcn$ ); the hexagonal structure previously suggested in computer simulations of  $\text{NaMgF}_3$  ( $P6_3/mmc$ ); the monoclinic structure found to be intermediate between the perovskite and  $\text{CaIrO}_3$  structures in  $\text{CaRhO}_3$  ( $P2_1/m$ ). Volumetric and axial equations of state of all phases considered are presented. For  $\text{KCaF}_3$ , as expected, the perovskite phase is shown to be the most thermodynamically stable at atmospheric pressure. With increasing pressure, the relative stability of the  $\text{KCaF}_3$  phases then follows the sequence: perovskite  $\rightarrow \text{La}_2\text{S}_3$  structure  $\rightarrow \text{Sb}_2\text{S}_3$  structure  $\rightarrow P6_3/mmc$  structure; the  $\text{CaIrO}_3$  structure is never the most stable form. Above about 2.6 GPa, however, none of the  $\text{KCaF}_3$  polymorphs are stable with respect to dissociation into  $\text{KF}$  and  $\text{CaF}_2$ . The possibility that high-pressure  $\text{KCaF}_3$  polymorphs might exist metastably at 300 K, or might be

stabilised by chemical substitution so as to occur within the standard operating range of a multi-anvil press, is briefly discussed. For  $\text{NaMgF}_3$ , the transitions to the high-pressure phases occur at pressures outside the normal range of a multi-anvil press. Two different sequences of transitions had previously been suggested from computer simulations. With increasing pressure, we find that the relative stability of the  $\text{NaMgF}_3$  phases follows the sequence: perovskite  $\rightarrow \text{CaIrO}_3$  structure  $\rightarrow \text{Sb}_2\text{S}_3$  structure  $\rightarrow P6_3/mmc$  structure. However, only the perovskite and  $\text{CaIrO}_3$  structures are stable with respect to dissociation into  $\text{NaF}$  and  $\text{MgF}_2$ .

**Keywords** Perovskite · Post-perovskite · Post–post-perovskite ·  $\text{KCaF}_3$  ·  $\text{NaMgF}_3$  · High pressure

## Introduction

If we are to have a proper understanding of the Earth's mantle, accurate determination of the physical properties of its constituent minerals is essential. For upper-mantle minerals, many of these properties are measurable directly in the laboratory, but the conditions of pressure and temperature that obtain in the lower mantle make such in situ studies increasingly challenging with increasing depth. In particular, experimental determination of the physical properties of the “post-perovskite (or “PPV”)” phase of  $\text{MgSiO}_3$ ,<sup>1</sup> which is thought to occur just above the Earth's core-mantle boundary in the D'' layer, presents a very severe challenge, as it

✉ Ian G. Wood  
ian.wood@ucl.ac.uk

<sup>1</sup> Laboratoire de Géologie de Lyon, Université Claude Bernard Lyon1, Ecole Normale Supérieure de Lyon, 46 allée d'Italie, 69342 Lyon Cedex 07, France

<sup>2</sup> Department of Earth Sciences, University College London, Gower Street, London WC1E 6BT, UK

<sup>1</sup> In this context, the term “perovskite (PV)” refers to the  $\text{GdFeO}_3$ -type structure (as found in the mineral bridgmanite; Tschauer et al. 2014) and the term “post-perovskite (PPV)” refers to the  $\text{CaIrO}_3$  structure (Rodi and Babel 1965).

is stable only at pressures in excess of about 100 GPa (see, e.g. Murakami et al. 2004; Oganov and Ono 2004; Tsuchiya et al. 2004; Shim et al. 2008; Tateno et al. 2009). It can be argued that the best way to address these difficulties is via a combination of computational and experimental studies. In this approach, experimental measurements are made on analogue phases, isostructural with the lower-mantle minerals, which are stable (or at least strongly metastable) at ambient pressure and temperature. These measurements may then be used to “ground truth” computer simulations of the analogue phases; if the agreement between experiment and simulations for the analogues proves satisfactory, and the simulations agree with experimental results on the natural system at lower pressures (if available), the computer simulations may then be applied to the natural system at high pressure with a high degree of confidence. As discussed below, two obvious examples of the need for this complementary method come from studies of the cation diffusivities in PPV-MgSiO<sub>3</sub> (where it has been reported from computer simulations that there is a directional anisotropy of a factor of about 10<sup>8</sup>, Ammann et al. 2010), and in confirming computer simulations of the possible high-pressure phases of MgSiO<sub>3</sub> under conditions relevant to the mantles of large terrestrial exoplanets (Umamoto et al. 2006a; Tsuchiya and Tsuchiya 2011).

When examining possible lower-mantle analogue phases, fluorides can be considered to have advantages over oxides as their high-pressure phases become stable at much lower pressures. For MgSiO<sub>3</sub> perovskite (bridgmanite), the mineral neighborite (NaMgF<sub>3</sub>) provides an obvious and attractive analogue (e.g. Umamoto et al. 2006b; Hustoft et al. 2008; Li and Weidner 2012), although other ABF<sub>3</sub> compounds such as KCaF<sub>3</sub> (Watson et al. 1995) and KZnF<sub>3</sub> (Poirier et al. 1983) have also been used for this purpose. NaMgF<sub>3</sub> may be readily synthesised at atmospheric pressure and is stable at atmospheric pressure and room temperature. At atmospheric pressure and room temperature it crystallises (e.g. Knight 2014), in common with many other compounds (e.g. Mitchell 2002), as an orthorhombically distorted perovskite, in what is commonly referred to as the gadolinium orthoferite structure (Geller 1956); the space group is *Pbnm* and the system of octahedral tilting producing the distortion from the cubic perovskite aristotype, for this setting of the space group, is  $a^-a^-c^+$  in the notation of Glazer (1972). NaMgF<sub>3</sub> is, therefore, isostructural with bridgmanite and the two compounds are also isoelectronic; in addition, the relative masses of the atoms in NaMgF<sub>3</sub> are not too dissimilar from those in MgSiO<sub>3</sub>. It is well known that NaMgF<sub>3</sub> undergoes a phase transition between the perovskite and CaIrO<sub>3</sub> structures (Martin et al. 2006a, b) and so this compound may also be used as an analogue for PPV-MgSiO<sub>3</sub> (e.g. Hustoft et al. 2008). In addition, on the basis of computer simulations, it has been suggested by Umamoto and Wentzcovitch (2006)

and by Xu et al. (2015) that further transitions in NaMgF<sub>3</sub> may occur at higher pressures, which may have some relevance to the mineralogy of super-earths (Umamoto et al. 2006a, b; Grocholski et al. 2010; Tackley et al. 2013). Umamoto and Wentzcovitch (2006) proposed that there would first be a transition from the CaIrO<sub>3</sub> phase to a lower-symmetry, orthorhombic structure, of the Sb<sub>2</sub>S<sub>3</sub> (stibnite) structure type (e.g. Lundegaard et al. 2003), as has now been found to occur by experiment in NaFeF<sub>3</sub> (Crichton et al. 2016) and in NaCoF<sub>3</sub> (Wood et al. 2017). At still higher pressure, Umamoto and Wentzcovitch (2006) found that a further transition occurred to a hexagonal structure with space group *P6<sub>3</sub>/mmc*, which does not seem to correspond to any known structure type; this hexagonal structure was considered by Crichton et al. (2016) to take the Be<sub>3</sub>N<sub>2</sub> structure (identical to that of InFeO<sub>3</sub> or InMnO<sub>3</sub>), but although these structures are isopointal (as their space group and occupied Wyckoff positions are the same; Allmann and Hinek 2007), they cannot be considered isoconfigurational as their axial ratios differ by an amount sufficient to cause changes in the primary coordination of the atoms. It should be noted, however, that Umamoto and Wentzcovitch (2006) also concluded that both of these new high-pressure phases would be metastable with respect to dissociation of NaMgF<sub>3</sub> into CsCl-structured NaF and cotunnite-structured MgF<sub>2</sub> (a similar sequence of transitions was predicted for CaSnO<sub>3</sub> by Tsuchiya and Tsuchiya 2006). In contrast, Xu et al. (2015) proposed a different high-pressure transition in NaMgF<sub>3</sub>, from the CaIrO<sub>3</sub> phase to a structure, with space group *Pnma*, that they termed “ppPv”, for “post-post-Perovskite”. Xu et al. (2015) stated that this structure “has never been previously reported in any material”, but it has since been pointed out by Crichton et al. (2016) that this “ppPv” phase actually corresponds to a structure of the La<sub>2</sub>S<sub>3</sub> type<sup>2</sup> (Besançon et al. 1969). Xu et al. (2015) considered that the simulated diffraction pattern of their La<sub>2</sub>S<sub>3</sub>-type structure for NaMgF<sub>3</sub> was consistent with the “N phase” reported to form at high pressure by Martin et al. 2006a, b, but they did not investigate its stability relative to the Sb<sub>2</sub>S<sub>3</sub>-type structure, nor did they examine its stability with respect to dissociation into NaF and MgF<sub>2</sub>.

In many respects, however, NaMgF<sub>3</sub> is a much less convenient analogue for PPV-MgSiO<sub>3</sub> than it is for the PV (bridgmanite) phase. The transition to the CaIrO<sub>3</sub> structure in NaMgF<sub>3</sub> occurs at between 28 and 30 GPa (Martin et al. 2006a), which is outside the standard range of a multi-anvil press, and although CaIrO<sub>3</sub>-type NaMgF<sub>3</sub> can be quenched to atmospheric pressure (Hustoft et al. 2008) some amorphisation of the high-pressure phases

<sup>2</sup> Crichton et al. (2016) refer to this structure as being identical to the  $\alpha$ -Gd<sub>2</sub>S<sub>3</sub> type, but in the Inorganic Crystal Structure Database (ICSD; Fletcher et al. 1996) this type structure is currently given as La<sub>2</sub>S<sub>3</sub>.

on decompression has also been reported (Martin et al. 2006a). For this reason, other  $ABF_3$  fluorides, such as  $NaCoF_3$  and  $NaNiF_3$  (Dobson et al. 2011; Shirako et al. 2012b; Yusa et al. 2012), which may be prepared in a multi-anvil press and then recovered to atmospheric pressure, where they remain quite strongly metastable, have been suggested as more suitable analogues for PPV- $MgSiO_3$ . These compounds have already proved to be of great value in experimental studies, in revealing the relative strength of PV and PPV polymorphs (Dobson et al. 2012), in demonstrating the topotaxial nature of the PV to PPV transition (Dobson et al. 2013), in determining the degree of anisotropy in the diffusion coefficients of the PPV phase (Dobson et al. 2014) and in allowing the determination of accurate PPV crystal structures (Lindsay-Scott et al. 2014).

A major disadvantage of the  $ABF_3$  fluorides, where  $A = Na$  and  $B =$  a first-row transition element, however, is that in the majority of these compounds the  $d$ -electrons of the  $B$  cation will have unpaired spins leading to magnetic ordering at low-temperatures. Bernal et al. (2014) have reported recently that PV- and  $CaIrO_3$ -type  $NaFeF_3$  show antiferromagnetic ordering at  $\sim 90$  and 48 K, respectively (with weak ferromagnetism observed in PV- $NaFeF_3$ ); similarly, PV- and  $CaIrO_3$ -type  $NaNiF_3$  order antiferromagnetically at 156 and 22 K, respectively (Shirako et al. 2012b) and the corresponding phases of  $NaCoF_3$  have antiferromagnetic transitions at 74 K (Friedman et al. 1970) and 24 K (A S Wills, pers. comm.). Although this magnetic ordering may be of little consequence for experiments carried out at room temperature, i.e. far above the Néel temperature, it does significantly complicate quantum mechanical simulations of these materials, as the correct magnetic ground state must be determined. For this reason we have been considering whether other  $ABF_3$  compounds, where  $A$  and  $B$  are cations from groups IA and IIA of the periodic table, can also form  $CaIrO_3$ -type polymorphs at high pressure. PV-structured compounds containing group IA and IIA cations are common, but to date only  $NaMgF_3$  has been found experimentally to form a phase isostructural with PPV- $MgSiO_3$ . Considering the most obvious examples,  $KMgF_3$ ,  $KCaF_3$  and  $RbCaF_3$ , it was thought unlikely that either  $KMgF_3$  (e.g. Wood et al. 2002) or  $RbCaF_3$  (e.g. Knight et al. 2014) would transform in this way as both are cubic perovskites at ambient pressure and temperature. This supposition is confirmed by studies at high pressure. For PV- $KMgF_3$ , it was found that the cubic structure is maintained to 50 GPa (Aguado et al. 2008). In contrast, PV- $RbCaF_3$  does undergo a lowering of symmetry with increasing pressure, but the transformation, at  $\sim 2.8$  GPa, is from a cubic to a tetragonal ( $I4/mcm$ ) perovskite; no further transformations were observed up to 7.9 GPa, the highest pressure reached in the experiment (Knight et al. 2014).

After  $NaMgF_3$ ,  $KCaF_3$  might appear to be one of the more promising candidate compounds, since at ambient pressure and temperature PV- $KCaF_3$  is also orthorhombically distorted with space group  $Pbnm$ . Furthermore, Fujino et al. (2009) have suggested (for oxides) that for PPV formation, the  $t$ -factor (Goldschmidt 1926; defined as  $t = (1/\sqrt{2})(R_A + R_F)/(R_B + R_F)$ , where  $R_X$  is an ionic radius) should lie in the range  $0.8 \leq t \leq 0.9$ ; for  $KCaF_3$ ,  $t = 0.862$ , almost identical to the value for  $NaMgF_3$ , 0.866 (ionic radii taken from Shannon 1976). A further requirement (derived from consideration of the behaviour of some  $A^{2+}B^{4+}O_3$  perovskites, together with that of  $NaMgF_3$ ) was suggested by Tateno et al. (2010) who proposed that for the  $CaIrO_3$  structure to form, the octahedral tilt in the PV phase at atmospheric pressure and room temperature,  $\Phi$ , estimated from the orthorhombic lattice parameters (in the  $Pbnm$  setting) by the relationship  $\Phi = \cos^{-1}(\sqrt{2}a^2/bc)$  (O'Keeffe and Hyde 1977) should be greater than  $13^\circ$ . For these oxides, and for  $NaMgF_3$ , it was found that application of pressure then led to an increase in  $\Phi$ , with the transition to the PPV structure occurring when  $\Phi$  exceeded  $19$ – $25^\circ$ . For  $NaMgF_3$ ,  $\Phi = 15.0^\circ$  at atmospheric pressure and 300 K (from the cell parameters given by Mitchell et al. 2007), but for  $KCaF_3$ ,  $\Phi = 9.3^\circ$  (Knight et al. 2005). This, however, does not necessarily rule out the possibility of the formation of  $CaIrO_3$ -type  $KCaF_3$  as: (1) the requirement is only a guide and (2) it is not yet known whether the conclusion that  $\Phi$  should be greater than about  $13^\circ$  is appropriate for fluorides, as opposed to oxides (indeed, the present work suggests that it may well not be, see “Equations of state for  $KCaF_3$  polymorphs and phase diagram of  $KCaF_3$ ”).

It is perhaps surprising that although there have been several crystallographic analyses of PV- $KCaF_3$  as a function of temperature (Knight et al. 2005; Mitchell et al. 2007; Knight 2009, 2011), very little has been published on the properties of  $KCaF_3$  at high pressure. Previous computational work has been confined to investigations of the effect of pressure on ionic conduction in PV- $KCaF_3$  by molecular dynamics simulations using interatomic potentials (Watson et al. 1992, 1995) and a recent quantum mechanical study of the effect of pressure on the band structure (Mousa 2014). No experimental high-pressure structural studies have as yet been published, but a number of such experiments have been carried out as part of, or associated with, our present study of  $KCaF_3$ . In the first of these, PV- $KCaF_3$  (provided by K S Knight and synthesised as described in Knight et al. 2005) was compressed to 15 GPa and held at this pressure for 24 h at 300 K in a multi-anvil press (MAP) at UCL; on recovery of the sample to atmospheric pressure it was found that it was still composed of PV- $KCaF_3$ . In further experiments using the MAP at UCL, PV- $KCaF_3$  was held at 5.5 GPa and 973 K for 220 min and at 14 GPa and 973 K for 8 h; on recovery to atmospheric pressure and room temperature both

samples were found to have decomposed to a mixture of KF and CaF<sub>2</sub>. As mentioned briefly in a paper on RbCaF<sub>3</sub> by Knight et al. (2014), KCaF<sub>3</sub> has been studied by neutron powder diffraction up to pressures of 6.86 GPa (at room temperature) on the PEARL beam line at the ISIS Facility of the Rutherford Appleton Laboratory, where it was found that the *Pbnm* perovskite structure was maintained throughout. Similar persistence of the *Pbnm* PV-structure throughout the experiment was also seen in a preliminary examination of KCaF<sub>3</sub> to ~20 GPa in a diamond-anvil cell (at room temperature) by synchrotron X-ray powder diffraction on beamline I15 at the Diamond Light Source.

In order to determine whether the failure to observe experimentally a CaIrO<sub>3</sub>-type phase of KCaF<sub>3</sub> was due to an inherent lack of stability or was merely a consequence of the pressure and temperature range covered in these few experiments, it was decided to supplement them with ab initio computer simulations. In this way we have been able to examine the relative stabilities in KCaF<sub>3</sub> of: (a) the four ABX<sub>3</sub> polymorphs described by Umemoto and Wentzcovitch (2006) for NaMgF<sub>3</sub>, (b) the “ppPv” (La<sub>2</sub>S<sub>3</sub>) structure reported by Xu et al. (2015), (c) the monoclinic phase found by Shirako et al. (2012a) as an intermediate between the PV and CaIrO<sub>3</sub> structures in CaRhO<sub>3</sub>, and also to determine the stability of these KCaF<sub>3</sub> compounds relative to a mixture of KF and CaF<sub>2</sub>. We have found that the PV phase of KCaF<sub>3</sub> is, as expected, the stable phase at atmospheric pressure but that at pressures in excess of about 2.6 GPa, none of the KCaF<sub>3</sub> structures are thermodynamically stable with respect to a mixture of KF and CaF<sub>2</sub>. In addition, as the sequence of phase transitions in NaMgF<sub>3</sub> predicted from ab initio simulations by Umemoto and Wentzcovitch (2006) and by Xu et al. (2015) differed, we also took this opportunity of carrying out a similar study of NaMgF<sub>3</sub>; we find that in NaMgF<sub>3</sub> the PV and CaIrO<sub>3</sub> structures are thermodynamically stable, but that none of the proposed higher-pressure phases are stable with respect to a mixture of NaF and MgF<sub>2</sub>.

## Computational method

The static ab initio calculations presented here used the projector augmented wave implementation (Blöchl 1994; Kresse and Joubert 1999) of the density functional theory (Hohenberg and Kohn 1964; Kohn and Sham 1965) with the generalised gradient approximation (GGA) PBE pseudopotentials (Perdew et al. 1996) implemented in the VASP computer code (Kresse and Furthmüller 1996; Kresse et al. 2010). For KCaF<sub>3</sub>, an electronic minimization convergence criterion of 10<sup>-6</sup> eV was used for the internal energy, with a *k*-point density of 4 × 4 × 4 (Monkhorst and Pack 1976) and a kinetic energy cutoff of 500 eV. For NaMgF<sub>3</sub>, the same electronic minimization convergence

criterion for the internal energy was used, but (for consistency with earlier work; Lindsay-Scott 2012) the *k*-point density was increased to 6 × 6 × 6 (Monkhorst and Pack 1976) and the kinetic energy cutoff to 900 eV.

The procedure adopted to determine the volumetric equation of state, and hence the enthalpy of each phase, was to use VASP to calculate the internal energy (*E*) of the crystal at a set of chosen volumes (*V*), allowing the cell parameters and the fractional coordinates (where necessary) to relax in accordance with the crystal symmetry. All simulations were made along a path of decreasing volume. During the calculations the program parameters were set such that the symmetry of the crystal was maintained. Transitions to structures with lower symmetry were, therefore, forbidden but transitions to structures whose space groups are supergroups could occur, as the atoms are not prevented from moving into a more symmetrical arrangement. Since the calculations were static and effectively equivalent to *T* = 0 K, the pressure (*P*) at any point on the *E* vs. *V* curve is given by the standard thermodynamic result  $P = -(\partial E/\partial V)_{T=0}$  (see, e.g. Pippard 1966), the actual values being determined by fitting the *E* (*V*) curve to an integrated Birch-Murnaghan 3rd-order equation of state (EoS; see, e.g. Vočadlo et al. 1999). Knowing *P*, *V* and *E*, the enthalpy, *H*, may be calculated. Since *T* = 0, the enthalpy is equal to the Gibbs free energy, *G*, and thus the most stable phase at any given pressure may be determined.

## Results and discussion

### General considerations

Initially, it was intended in this study to consider only the relative stabilities of the PV- and CaIrO<sub>3</sub>-phases of KCaF<sub>3</sub>. It was found, however, see Fig. 1, that when the volume of the unit cell of PV-KCaF<sub>3</sub> was reduced below about 280 Å<sup>3</sup> (~17 GPa) a spontaneous transition occurred in the simulations, leading to a different crystal structure. Inspection of the resulting fractional coordinates, using the crystal structure plotting package *Diamond* (Putz and Brandenburg 2006), revealed that this structure corresponded to the hypothetical high-pressure hexagonal phase of NaMgF<sub>3</sub> (space group *P6<sub>3</sub>/mmc*) previously described by Umemoto and Wentzcovitch (2006); in this structure, which does not appear yet to have been observed experimentally, the B cations are [8]-coordinated by the anions. The occurrence of this transition then led us to consider three further possible structures, as follows: (1) the Sb<sub>2</sub>S<sub>3</sub>-structured phase of NaMgF<sub>3</sub> with space group *Pmcn* (Umemoto and Wentzcovitch 2006), containing B cations sevenfold coordinated by the anions (as observed recently in NaFeF<sub>3</sub> and NaCoF<sub>3</sub> above ~22 GPa in synchrotron X-ray diffraction

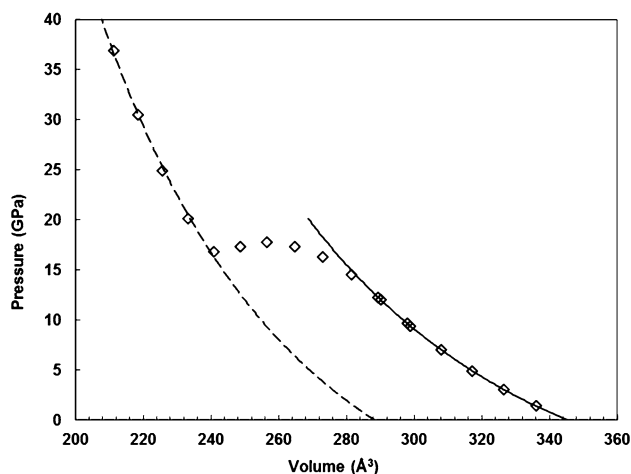


**Fig. 1** Pressure versus volume for  $\text{KCaF}_3$  obtained by compression of the  $Pbnm$  perovskite structure. The pressure values at the simulation points (symbols) are taken from the VASP output; the lines show Birch–Murnaghan 3rd-order equations of state, fitted to  $P(V)$ . The transition from the PV to the  $P6_3/mmc$ - $\text{NaMgF}_3$  structure can be clearly seen

experiments at room temperature by Crichton et al. 2016 and Wood et al. 2017); (2) the  $\text{La}_2\text{S}_3$ -structured phase found by Xu et al. (2015); (3) the monoclinic ( $P2_1/m$ ) “intermediate phase” reported by Shirako et al. (2012a) for  $\text{CaRhO}_3$ .<sup>3</sup> The PV,  $\text{Sb}_2\text{S}_3$  and  $\text{La}_2\text{S}_3$  structures are isosymmetric, but in order to more readily understand the relationship between the structures, it is convenient to use the  $Pbnm$  setting of their space group for the PV phase and the  $Pmcn$  setting for the  $\text{Sb}_2\text{S}_3$  and  $\text{La}_2\text{S}_3$ -structured phases; the space group of the  $\text{CaIrO}_3$  structure is  $Cmcm$ . The symmetry relationships between these structures are interesting in that  $Cmcm$  is a supergroup of  $Pbnm$  and thus symmetry is increased in a PV to  $\text{CaIrO}_3$ -type transition; the symmetry then reduces on

<sup>3</sup> Following the “perovskite > post-perovskite” terminology it is tempting to refer to any higher-pressure phases as “post-post-perovskite” or even “post-post-post-perovskite”, as has been done in the past by others. However, acting on admirable advice from Wilson Crichton (pers. comm.) and an anonymous reviewer, we now believe that it is far better to use structure-type labels whenever possible. The succession of phases following the perovskite structure at high pressures has now been found to differ for different  $\text{ABX}_3$  compounds (e.g. Shirako et al. 2012a; Xu et al. 2015) and so there can now be confusion as to what is implied by, e.g. a “post-post-perovskite structure”. We have, though, retained the term “perovskite” instead of “ $\text{GdFeO}_3$ -type” as this term is in such common usage. Similarly, in the case of  $\text{MgSiO}_3$ , the term “post-perovskite” has been retained as indicating the  $\text{CaIrO}_3$ -type structure. One of the structures that we consider here, that with space group  $P6_3/mmc$  (Umemoto and Wentzcovitch 2006) does not seem to have been observed experimentally and so we refer to this as the “ $P6_3/mmc$ - $\text{NaMgF}_3$  structure”. Similarly, we refer to the monoclinic ( $P2_1/m$ ) “intermediate phase” of Shirako et al. (2012a) as the “ $P2_1/m$ - $\text{CaRhO}_3$  structure”, as this has no structure type in the ICSD (Fletcher et al. 1996).

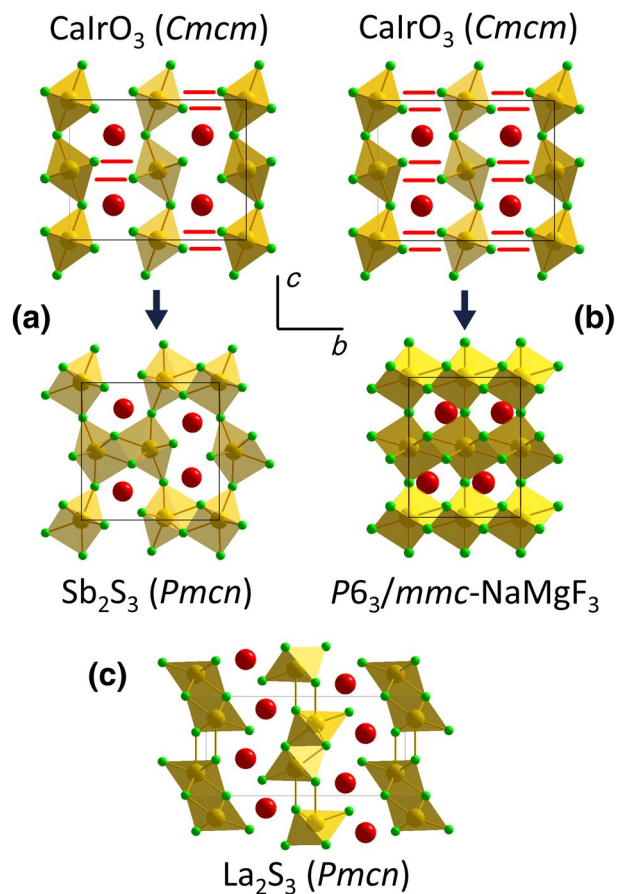


**Fig. 2** The structural mechanism for the transformations between **a** the  $\text{CaIrO}_3$  and  $\text{Sb}_2\text{S}_3$  structures and **b** the  $\text{CaIrO}_3$  and  $P6_3/mmc$ - $\text{NaMgF}_3$  structures (after Umemoto and Wentzcovitch 2006); **c** the  $\text{La}_2\text{S}_3$  structure of  $\text{NaMgF}_3$  (coordinates from Xu et al. 2015, transformed to the  $Pmcn$  setting). The A-cations are shown in red, the B-cations in gold and the anions in green. The structures are viewed along the orthorhombic  $a$ -axis, with the orthorhombic  $b$ - and  $c$ -axes as marked; so as to enable ready comparison with the  $\text{CaIrO}_3$  and  $\text{Sb}_2\text{S}_3$  structures, the hexagonal  $P6_3/mmc$ - $\text{NaMgF}_3$  structure is represented here using a  $C$ -centred unit cell with an orthorhombic metric in which  $b = \sqrt{3}a$ . In **c** the coordination polyhedra are drawn as octahedra; there is a 7th Mg–F distance nearly parallel to the  $c$ -axis (shown here as a bond) which is only slightly longer; for details see text

transformation to either the  $\text{Sb}_2\text{S}_3$  or  $\text{La}_2\text{S}_3$ -phases, but rises once more in the  $P6_3/mmc$ - $\text{NaMgF}_3$  structure as  $P6_3/mmc$  is a supergroup of  $Cmcm$  (and thus also of  $Pmcn$ ).

The structural relationship between the  $\text{CaIrO}_3$ ,  $\text{Sb}_2\text{S}_3$  and  $P6_3/mmc$ - $\text{NaMgF}_3$  phases in an  $\text{ABF}_3$  compound is readily understood from Fig. 2a, b (after Umemoto and Wentzcovitch 2006). Starting from the  $\text{CaIrO}_3$  structure, the  $\text{Sb}_2\text{S}_3$  structure can be envisaged as forming with increasing pressure in the following way. The  $\text{CaIrO}_3$ -type structure contains two-dimensional sheets of edge and corner linked  $\text{BF}_6$  octahedra lying perpendicular to the  $b$ -axis. As the  $b$ -axis (the most easily compressible of the three, see

Table 2) shortens on compression,  $F^-$  ions enter the primary coordination shell of B ions in adjacent sheets of octahedra, thereby linking alternating pairs of  $BF_6$  octahedra, and increasing the primary coordination of all of the B cations from 6 to 7 (Fig. 2a). The  $P6_3/mmc$ - $NaMgF_3$  structure then forms by a similar mechanism, whereby further reduction of the axial ratio  $b/a$  to  $\sqrt{3}$  and linkage of all octahedra (rather than just alternating pairs) by  $F^-$  ions from adjacent sheets leads to a structure with hexagonal symmetry and B ions in [8]-fold coordination by F (Fig. 2b).

The transition between the  $CaIrO_3$  and  $La_2S_3$ -structures (Xu et al. 2015) is quite different in that the sheets of edge and corner linked  $BF_6$  octahedra found in the  $CaIrO_3$  structure are disrupted. With space group setting  $Pm\bar{c}n$  for the  $La_2S_3$  phase of  $NaMgF_3$ , there is a direct correspondence between the axes of the unit-cell of these two structures. Xu et al. (2015) found that on forming the  $La_2S_3$  structure the  $b$ -axis of  $CaIrO_3$ -type  $NaMgF_3$  expanded by ~25%, whilst the  $c$ -axis contracted by a similar percentage; the  $a$ -axis shows about a 4% expansion. It is, therefore, difficult to envisage formation of the  $La_2S_3$  phase by hydrostatic compression of a  $CaIrO_3$ -type structure in a real material, as in all such structures for which axial incompressibilities have been measured to date (e.g. Boffa Ballaran et al. 2007; Lindsay-Scott et al. 2010; Wood et al. 2017) the  $b$ -axis has been found to be considerably more compressible than either  $a$ - or  $c$ -axes. Figure 2c shows the  $La_2S_3$  structure, which can perhaps be considered to form in the following way. As the  $c$ -axis shortens, the tilt of the corner-linked octahedra (the angle  $\Delta_1$  in Lindsay-Scott et al. 2011) increases until a point is reached at which the sheets of octahedra cannot be maintained and alternating double rods of edge-linked octahedra running parallel to the  $a$ -axis are formed. Whether these rods are then considered to be linked along the  $c$ -axis, depends on whether the B cation is considered to be in sixfold or sevenfold coordination; from the coordinates published by Xu et al. (2015), we find 6 Mg–F distances in the range 1.81–1.94 Å and one slightly longer distance—the Mg–F bond closely parallel to the  $c$ -axis in Fig. 2c—of 2.10 Å.

### Equations of state for $KCaF_3$ polymorphs and phase diagram of $KCaF_3$

Table 1 shows the volumetric equation of state (EoS) parameters, derived from fitting  $E(V)$ , for the PV,  $P2_1/m$ - $CaRhO_3$ ,  $CaIrO_3$ ,  $La_2S_3$ ,  $Sb_2S_3$  and  $P6_3/mmc$ - $NaMgF_3$  phases of  $KCaF_3$ , together with those for the relevant phases of KF and  $CaF_2$ . In the pressure range of interest, 0 to ~30 GPa, KF undergoes a transition from the NaCl to the CsCl structures (Weir and Piermarini 1964); similarly, the parameters for  $CaF_2$  in both the low-pressure fluorite and high-pressure cotunnite structures (Wu et al. 2006) are given. The axial EoS parameters for the non-cubic phases,

derived from fitting 2nd-order Birch–Murnaghan EoS to the VASP output pressure versus volume, using the program EoSFit (Angel 2001) are given in Table 2. To enable ready comparison with the volumetric EoS, the values of  $K_0$  listed in this table are those obtained by fitting the cubes of the lengths of the unit-cell edges; a 2nd-order Birch–Murnaghan EoS was used here as the uncertainties in some of the fitted parameters would otherwise have been very high. The axial EoS for PV- $KCaF_3$  allows the macroscopic tilt angle,  $\Phi$ , to be calculated as a function of pressure. When calculated on this basis,  $\Phi$  rises from 10.1° at zero pressure to 16.1° at a pressure of 10 GPa, suggesting either that the relationship proposed by Tateno et al. (2010—see above) does not apply to the  $ABF_3$  perovskites, or that the minimum value of  $\Phi$ , above which  $\Phi$  will increase with pressure, is less than that for the  $A^{2+}B^{4+}O_3$  oxide perovskites. A second feature of the axial EoS shown in Table 2 is the extreme anisotropy of the  $CaIrO_3$ -type phase of  $KCaF_3$  and the very low incompressibility (8 (2) GPa) of its  $b$ -axis. As discussed above, the likely mechanism for the formation of the  $Sb_2S_3$  and  $P6_3/mmc$ - $NaMgF_3$  phases requires the  $b$ -axis to be the most compressible so as to reduce the distance between the sheets of  $BF_6$  octahedra and enable them to cross-link. In  $KCaF_3$ , however, the value of the incompressibility of the  $b$ -axis is so low as to suggest that the  $CaIrO_3$  structure may not be stable with respect to formation of the  $La_2S_3$ , or  $Sb_2S_3$  polymorphs, as is indeed found to be the case (see below).

The enthalpies derived from the EoS parameters listed in Table 1 are shown in Fig. 3, relative to that of  $CaIrO_3$ -structured  $KCaF_3$ . Considering first just the  $KCaF_3$  polymorphs themselves, it can be seen that a transition from the PV to the  $La_2S_3$  structures might be expected at about 5.7 GPa, followed by further transitions to the  $Sb_2S_3$  structure at around 10.4 GPa and to the  $P6_3/mmc$ - $NaMgF_3$  structure at 28.3 GPa, confirming our original prejudice that PV- $KCaF_3$  might be expected to transform at relatively low pressures. However, Fig. 3 also shows that the  $CaIrO_3$  structure does not appear to be the relatively most stable polymorph of  $KCaF_3$  at any pressure. Although we did not expect this result prior to the simulations, it is quite consistent with simple crystal-chemical considerations based on ionic sizes, as the large  $Ca^{2+}$  ion is readily able to support coordination numbers higher than six. At atmospheric pressure, the radius ratios of the B cations (in [6]—coordination; Shannon 1976) to the  $F^-$  ions are 0.541 for Mg/F and 0.752 for Ca/F. The value for  $NaMgF_3$  thus lies firmly within the range expected for octahedral coordination (0.414–0.732; Pauling 1929). For  $KCaF_3$ , however, the value lies slightly outside this range and just within the range for which a higher coordination number might be expected; on purely geometric grounds, radius ratios in the range 0.732–1.0 are sufficient to support [8]-fold cubic coordination. The  $CaF_6$  octahedra

**Table 1** Equation of state parameters for  $\text{KCaF}_3$ ,  $\text{KF}$  and  $\text{CaF}_2$  polymorphs obtained by fitting the internal energy versus volume to integrated 3rd-order Birch–Murnaghan equations of state

	$V_0$ ( $\text{\AA}^3$ )	$K_0$ (GPa)	$K'_0$	$E_0$	Volume range fitted ( $\text{\AA}^3$ )	Transition to next phase (GPa)
$\text{KCaF}_3$ (PV)	348.62 (6)	44.9167 (5)	4.63 (5)	−104.351 (1)	290–408	5.7 to $\text{La}_2\text{S}_3$
$\text{KCaF}_3$ ( $P2_1/m$ - $\text{CaRhO}_3$ )	336.1 (7)	45.477 (7)	3.36 (7)	−103.68 (1)	320–510	5.4 to $\text{Sb}_2\text{S}_3$
$\text{KCaF}_3$ ( $\text{CaIrO}_3$ )	347.0 (6)	35.033 (4)	4.03 (5)	−103.72 (2)	185–413	0.23 to $\text{La}_2\text{S}_3$
$\text{KCaF}_3$ ( $\text{La}_2\text{S}_3$ )	328.7 (8)	48.260 (8)	3.24 (8)	−103.69 (1)	210–340	10.4 to $\text{Sb}_2\text{S}_3$
$\text{KCaF}_3$ ( $\text{Sb}_2\text{S}_3$ )	316.6 (2)	50.246 (4)	4.47 (6)	−103.115 (2)	230–320	28.3 to $P6_3/mmc$ - $\text{NaMgF}_3$
$\text{KCaF}_3$ ( $P6_3/mmc$ - $\text{NaMgF}_3$ )	300.739 (7)	52.1206 (2)	4.709 (4)	−101.0631 (3)	218–336	–
$\text{KF}$ ( $\text{NaCl}$ )	160.24 (9)	29.440 (2)	4.72 (8)	−33.7269 (5)	128–158	7.3 to $\text{KF}(\text{CsCl})$
$\text{KF}$ ( $\text{CsCl}$ )	139.36 (2)	32.9110 (7)	4.83 (2)	−32.9049 (1)	106–140	–
$\text{CaF}_2$ (fluorite)	168.7 (1)	75.60 (1)	4.8 (3)	−70.307 (1)	148–166	7.9 to $\text{CaF}_2$ (cotunnite)
$\text{CaF}_2$ (cotunnite)	155.60 (6)	72.299 (4)	4.85 (8)	−69.6767 (6)	128–148	–

The volume ranges used were chosen so as to eliminate a few higher-pressure data points with larger energy residuals from the fit. The volumes refer to unit cells containing 4 formula units: the  $V_0$  and  $E_0$  parameters for  $P2_1/m$  have been scaled from 6 to 4 formula units

The dissociation of  $\text{KCaF}_3$  PV to  $\text{CaF}_2$  (fluorite) and  $\text{KF}$  ( $\text{NaCl}$ ) takes place at 2.62 GPa

The sequences of phase transitions in the simple fluorides were taken from Weir and Piermarini (1964) for  $\text{KF}$ , and from Wu et al. (2006) for  $\text{CaF}_2$

**Table 2** Volumetric and axial equation of state (EoS) parameters for  $\text{KCaF}_3$  and  $\text{CaF}_2$  polymorphs obtained by fitting pressure (as output by VASP) versus volume to 2nd-order Birch–Murnaghan EoS (Angel 2001); the volume range used in each case are shown

	Volume		$a$ -axis		$b$ -axis		$c$ -axis	
	$V_0$ ( $\text{\AA}^3$ )	$K_0$ (GPa)	$a_0$ ( $\text{\AA}$ )	$K_0$ (GPa)	$b_0$ ( $\text{\AA}$ )	$K_0$ (GPa)	$c_0$ ( $\text{\AA}$ )	$K_0$ (GPa)
$\text{KCaF}_3$ (PV) (298–346 $\text{\AA}^3$ )	345.36 (7)	48.6 (1)	6.22 (1)	39 (1)	6.301 (4)	62 (2)	8.821 (3)	47.8 (5)
$\text{KCaF}_3$ ( $P2_1/m$ - $\text{CaRhO}_3$ ) (320–510 $\text{\AA}^3$ )	505 (2)	37.2 (6)	14.63 (4)	26 (2)	3.564 (5)	95 (8)	9.81 (1)	38.6 (7)
$\text{KCaF}_3$ ( $\text{CaIrO}_3$ ) (276.55–340.45 $\text{\AA}^3$ )	341.2 (7)	38.5 (7)	3.47 (1)	73 (6)	12.1 (2)	8 (2)	8.36 (1)	118 (21)
$\text{KCaF}_3$ ( $\text{La}_2\text{S}_3$ ) (260–300 $\text{\AA}^3$ )	327.3 (2)	43.5 (3)	3.61 (1)	100 (11)	14.42 (5)	21 (1)	6.31 (1)	50 (2)
$\text{KCaF}_3$ ( $\text{Sb}_2\text{S}_3$ ) (220–305 $\text{\AA}^3$ )	312.4 (3)	56.6 (4)	3.62 (1)	81 (5)	9.46 (4)	34 (3)	9.16 (2)	66 (4)
$\text{KCaF}_3$ ( $P6_3/mmc$ - $\text{NaMgF}_3$ ) (218.43–298.95 $\text{\AA}^3$ )	296.3 (6)	61.6 (8)	4.237 (2)	67.6 (7)	7.337 (5)	68 (1)	9.533 (8)	51.4 (8)
$\text{CaF}_2$ (cotunnite) (128–152.74 $\text{\AA}^3$ )	154.0 (2)	81.3 (9)	6.020 (3)	72 (1)	3.631 (3)	64 (1)	7.06 (2)	117 (4)

To enable ready comparison with the volumetric EoS, the values of  $K_0$  listed in the table are those obtained by fitting the cubes of the lengths of the unit-cell edges. In view of the large uncertainties in some of the fitted parameters the 2nd-order, rather than the 3rd-order Birch–Murnaghan EoS was used. The volumes refer to unit cells containing 4 formula units

So as to enable ready comparison with the  $\text{CaIrO}_3$  and  $\text{Sb}_2\text{S}_3$  structures, the hexagonal  $P6_3/mmc$ - $\text{NaMgF}_3$  structure is represented here using a  $C$ -centred unit cell with an orthorhombic metric in which  $b = \sqrt{3}a$ ; the symmetry also requires the value of  $K_0$  for these two axes to be the same. In constructing the Table, the  $a$ - and  $b$ -axes were fitted independently; the small deviations of the fitted parameters from the relationships expected from the symmetry are not significant

found in PV- $\text{KCaF}_3$  must, therefore, be almost at the limit of stability. When pressure is applied to  $\text{KCaF}_3$  and  $\text{NaMgF}_3$  it is to be expected that these radius ratios will increase, as the  $\text{F}^-$  ions will be more compressible than the cations. On compression, therefore,  $\text{KCaF}_3$  may quickly reach the point

where octahedral coordination will no longer be stable and thus the  $\text{La}_2\text{S}_3$  and  $\text{Sb}_2\text{S}_3$  structures, in which the coordination will be sevenfold, or almost sevenfold, will form. For  $\text{NaMgF}_3$  (Fig. 4 and see below) this point is not reached until much higher pressure and so there is a stable region of the

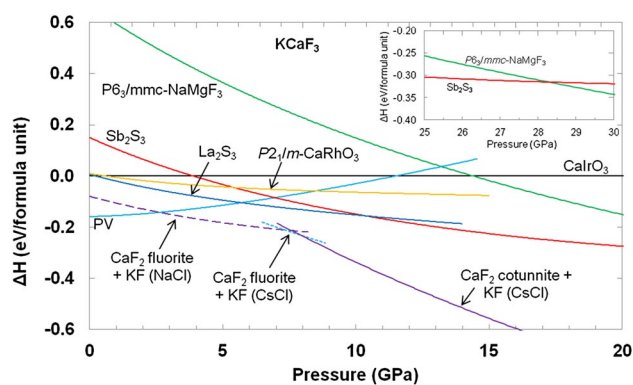


**Fig. 3** Enthalpies of the PV,  $P2_1/m$ -CaRhO<sub>3</sub>, La<sub>2</sub>S<sub>3</sub>, Sb<sub>2</sub>S<sub>3</sub> and  $P6_3/mmc$ -NaMgF<sub>3</sub> polymorphs of KCaF<sub>3</sub> relative to that of KCaF<sub>3</sub> in the CaIrO<sub>3</sub> structure. The relative enthalpies of mixtures of the simple fluorides are also shown. The lines for the Sb<sub>2</sub>S<sub>3</sub> and  $P6_3/mmc$ -NaMgF<sub>3</sub> polymorphs cross at 28.3 GPa

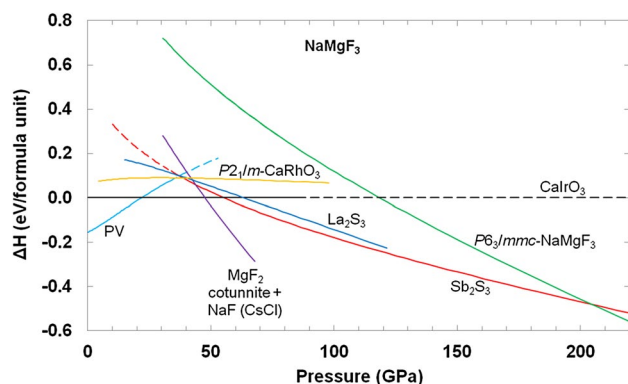


**Fig. 4** Enthalpies of the PV,  $P2_1/m$ -CaRhO<sub>3</sub>, La<sub>2</sub>S<sub>3</sub>, Sb<sub>2</sub>S<sub>3</sub> and  $P6_3/mmc$ -NaMgF<sub>3</sub> polymorphs of NaMgF<sub>3</sub> relative to that of NaMgF<sub>3</sub> in the CaIrO<sub>3</sub> structure. The relative enthalpies of mixtures of the simple fluorides are also shown

CaIrO<sub>3</sub> phase, which has a higher density than the PV phase and in which the structure still contains MgF<sub>6</sub> octahedra.

However, when the enthalpies of the KCaF<sub>3</sub> polymorphs are considered relative to that of a mixture of KF and CaF<sub>2</sub>, Fig. 3 also shows that the PV structure is the only polymorph of KCaF<sub>3</sub> that is ever the thermodynamically most stable phase, and that this is the case only at low pressures. Above about 2.6 GPa, none of the other polymorphs considered are predicted to be stable with respect to dissociation into KF and CaF<sub>2</sub>. The simulations presented here are static and so are effectively athermal, but it seems unlikely that consideration of temperature will significantly affect the thermodynamic stability of the KCaF<sub>3</sub> phases relative to dissociation into the simple fluorides, since, for example, Fig. 3 shows that by ~7 GPa the enthalpy difference, which increases with increasing pressure, is already about 100 meV per formula unit. It is possible, however, that the high-pressure KCaF<sub>3</sub>

structures could be synthesised by metastable compression in the diamond-anvil cell, since the dissociation reaction requires diffusion of atoms on the multi-unit-cell length scale, which will have a large energy barrier, whereas the structural transitions between the KCaF<sub>3</sub> phases require no long-range atomic movements and should have much smaller energy barriers. Indeed, the spontaneous transition from the PV to  $P6_3/mmc$ -NaMgF<sub>3</sub> structures found in the computer simulations suggests that there is no energy barrier to this transition. Support for this view comes from our recent study of NaCoF<sub>3</sub> by synchrotron X-ray powder diffraction in a diamond anvil cell, where we found that at 300 K the Sb<sub>2</sub>S<sub>3</sub> phase of NaCoF<sub>3</sub> formed at ~23 GPa and persisted to pressures of at least 85 GPa (Wood et al. 2017). In contrast, Yusa et al. (2012) found that, on heating, NaCoF<sub>3</sub> disproportionated into Na<sub>5</sub>Co<sub>3</sub>F<sub>11</sub> and NaCo<sub>3</sub>F<sub>7</sub> at ~20 GPa and 1400 K, with a negative Clapeyron slope, which implies that NaCoF<sub>3</sub> should not be stable (with respect to other complex stoichiometries) by about 28 GPa at 300 K.

The two unpublished in situ high-pressure experimental studies that have been carried out to date are insufficient to determine whether or not any metastable high-pressure phases of KCaF<sub>3</sub> exist. In the case of the neutron diffraction study by Knight et al. (2014), it has been confirmed (K S Knight, pers. comm.) that no decomposition products or phase transitions were observed in the range of the experiment, i.e. for pressures ≤6.86 GPa. This pressure is just greater than that at which the transition from the PV to the La<sub>2</sub>S<sub>3</sub> phase is predicted to occur in our simulations, but when the likely slope of the phase boundary is taken into consideration it may not be sufficient. For NaCoF<sub>3</sub>, the slope of the PV/PPV boundary has been determined to be 15.5 MPa K<sup>-1</sup> (Dobson et al. 2011); if a similar slope is assumed for the PV/La<sub>2</sub>S<sub>3</sub> boundary in KCaF<sub>3</sub>, the transition pressure at 300 K rises to ~10.5 GPa, well above that achieved in the neutron diffraction study. Persistence of PV-KCaF<sub>3</sub> to still higher pressures has been observed ex situ at 300 K in a sample recovered from 15 GPa in our multi-anvil press and also in our in situ diamond-anvil cell study, which showed PV-KCaF<sub>3</sub> persisting to 20 GPa. However, the fact that no transition to the La<sub>2</sub>S<sub>3</sub> or Sb<sub>2</sub>S<sub>3</sub> structures was seen in this experiment does not necessarily mean that the  $P6_3/mmc$ -NaMgF<sub>3</sub> structure will not form at higher pressures, as it is the transition from the PV to  $P6_3/mmc$ -NaMgF<sub>3</sub> structures that we have observed to occur spontaneously in our computer simulations. Taking account of the slope of the phase boundary, as above, we might expect this transition to occur at ~33 GPa, considerably higher than the maximum pressure of the experiment. We consider, therefore, that a study of KCaF<sub>3</sub> to ~50 GPa might well be rewarding, since if the  $P6_3/mmc$ -NaMgF<sub>3</sub> polymorph of KCaF<sub>3</sub> does form on further compression we believe that this would be the first occurrence of this structure.



**Table 3** Equation of state parameters for NaMgF<sub>3</sub>, NaF and MgF<sub>2</sub> polymorphs obtained by fitting the internal energy versus volume to integrated 3rd-order Birch–Murnaghan equations of state

	$V_0$ (Å <sup>3</sup> )	$K_0$ (GPa)	$K'_0$	$E_0$	Volume range fitted (Å <sup>3</sup> )	Transition to next phase (GPa)
NaMgF <sub>3</sub> (PV)	235.73 (6)	69.801 (2)	3.94 (2)	−99.1497(8)	175–235	21.9 to CaIrO <sub>3</sub>
NaMgF <sub>3</sub> ( <i>P2<sub>1</sub>/m</i> -CaRhO <sub>3</sub> )	234.6 (2)	57.557 (2)	4.55 (1)	−98.281(5)	140–220	38.7 to Sb <sub>2</sub> S <sub>3</sub>
NaMgF <sub>3</sub> (CaIrO <sub>3</sub> )	232.38 (7)	61.504 (1)	4.49 (1)	−98.527(1)	145–234	55.1 to Sb <sub>2</sub> S <sub>3</sub>
NaMgF <sub>3</sub> (La <sub>2</sub> S <sub>3</sub> )	233.2 (6)	55.635 (6)	4.52 (3)	−97.77(3)	130–195	36.7 to Sb <sub>2</sub> S <sub>3</sub>
NaMgF <sub>3</sub> (Sb <sub>2</sub> S <sub>3</sub> )	218.7 (3)	78.153 (4)	4.31 (1)	−96.55(3)	105–170	204.7 to <i>P6<sub>3</sub>/mmc</i> -NaMgF <sub>3</sub>
<i>P6<sub>3</sub>/mmc</i> -NaMgF <sub>3</sub>	211.9 (3)	84.751 (4)	4.270 (8)	−93.96(2)	100–170	–
NaF (CsCl)	93.96 (4)	49.7683 (8)	4.524 (3)	−33.336(2)	49–71	–
MgF <sub>2</sub> (cotunnite)	119.6 (1)	86.542 (7)	4.83 (5)	−61.350(6)	85–105	–

The volumes refer to unit cells containing 4 formula units: the  $V_0$  and  $E_0$  parameters for *P2<sub>1</sub>/m* have been scaled from 6 to 4 formula units

The dissociation of CaIrO<sub>3</sub>-type NaMgF<sub>3</sub> to MgF<sub>2</sub> (cotunnite) and NaF (CsCl) takes place at 47.6 GPa

A further possibility would be to determine whether (K, Na)(Ca, Mg)F<sub>3</sub> solid solutions could provide an alternative route to the various high-pressure structures. Although NaCaF<sub>3</sub> itself does not appear to exist (at least at atmospheric pressure), doping KCaF<sub>3</sub> with Na should lead to a substantial reduction in the average size of the A cation, which, in the case of the CaIrO<sub>3</sub> structure, will produce a substantial reduction in the length of the *b*-axis but only minor changes in the *a*- and *c*-axes. An estimate of the magnitude of these changes can be obtained by considering the CaIrO<sub>3</sub> structure parameterised in terms of the four shortest cation–anion distances and three tilt angles, as suggested by Lindsay-Scott et al. (2011; Equations 4–6). By putting the interatomic distances equal to the sum of the ionic radii (Shannon 1976), and assuming the same tilt angles as in NaNiF<sub>3</sub> (Lindsay-Scott et al. 2014), we obtain  $a = 3.48$  Å,  $b = 12.12$  Å and  $c = 8.67$  Å for CaIrO<sub>3</sub>-type KCaF<sub>3</sub> at  $P = 0$ , in good agreement with the cell parameters obtained by fitting the axial EoS to the VASP simulations ( $a = 3.47$  (1) Å,  $b = 12.1$  (2) Å and  $c = 8.36$  (1) Å). If the AF distance is now reduced to that appropriate for a composition of K<sub>0.5</sub>Na<sub>0.5</sub>CaF<sub>3</sub>, a value of  $b = 11.00$  Å then results ( $a$  and  $c$  are unchanged in this approximation), which is equivalent to applying a pressure of ~4.1 GPa. It thus seems quite possible that a combination of applied pressure and chemical substitution might well lead to the formation of the high-pressure KCaF<sub>3</sub> phases under relatively easily accessible experimental conditions.

### Equations of state for NaMgF<sub>3</sub> polymorphs and phase diagram of NaMgF<sub>3</sub>

The equation of state parameters for the NaMgF<sub>3</sub>, NaF and MgF<sub>2</sub> polymorphs are listed in Table 3 and the corresponding enthalpy curves are shown in Fig. 4. Considering first just the NaMgF<sub>3</sub> phases, it can be seen that the predicted

sequence of transitions, with increasing pressure (transition pressures in brackets), is PV to CaIrO<sub>3</sub> (~22 GPa), CaIrO<sub>3</sub> to Sb<sub>2</sub>S<sub>3</sub> (~55 GPa) and Sb<sub>2</sub>S<sub>3</sub> to *P6<sub>3</sub>/mmc*-NaMgF<sub>3</sub> (~205 GPa). Our results are, therefore, in good accord with those of Umemoto and Wentzcovitch (2006) who found the same sequence of transitions, occurring at about 18, 44 and 223 GPa. Conversely, Xu et al. (2015) found the sequence PV to CaIrO<sub>3</sub> (~19 GPa), followed by CaIrO<sub>3</sub> to La<sub>2</sub>S<sub>3</sub> (~51 GPa). All three studies agree in that they indicate a fairly wide phase field (~30 GPa) for the CaIrO<sub>3</sub> structure, reflecting the ability of the Mg ions to remain in octahedral coordination to higher pressures (see above). Although the stable phase at pressures above ~55 GPa predicted by Xu et al. (2015) differs from the Sb<sub>2</sub>S<sub>3</sub> structures found by Umemoto and Wentzcovitch (2006) and in the present study, it should be pointed out that the difference in enthalpy is small, being less than 10 meV/atom, and so the sequence of phases might differ at finite temperatures. There is, however, now strong experimental evidence, including crystal structure refinements, for the formation of Sb<sub>2</sub>S<sub>3</sub> structures in some ABF<sub>3</sub> compounds, as essentially phase-pure samples have been reported for NaFeF<sub>3</sub> by Crichton et al. (2016) and for NaCoF<sub>3</sub> by Wood et al. (2017). The experimental evidence for the formation of the La<sub>2</sub>S<sub>3</sub> structure is, at present, much weaker. Xu et al. (2015) considered that their simulated powder diffraction pattern of La<sub>2</sub>S<sub>3</sub>-structured NaMgF<sub>3</sub> resembled that of the “N phase” reported by Martin et al. (2006a), but the space group and unit-cell parameters suggested by Martin et al. are different. Martin et al. (2006a) have space group *Pnmm* and experimental unit-cell parameters of  $a = 8.353$  (3) Å,  $b = 5.265$  (2) Å,  $c = 5.857$  (3) Å,  $V = 257.58$  (3) Å<sup>3</sup> at 37 (1) GPa, whereas Xu et al. (2015) have space group *Pnma*, with  $a = 5.082$  Å,  $b = 2.829$  Å,  $c = 10.215$  Å,  $V = 146.9$  Å<sup>3</sup> for their simulation of the La<sub>2</sub>S<sub>3</sub> structure at 60 GPa. Correspondence of the “N phase” of Martin et al. (2006a) with the La<sub>2</sub>S<sub>3</sub> structure would,

therefore, seem to imply that the experimental powder pattern has been mis-indexed.

When the enthalpies of the NaMgF<sub>3</sub> polymorphs are considered relative to that of a mixture of NaF and MgF<sub>2</sub>, however, Fig. 4 shows that only the PV and CaIrO<sub>3</sub> structures will be the thermodynamically most stable phases. For pressures above ~48 GPa we find that all NaMgF<sub>3</sub> polymorphs are unstable with respect to dissociation into NaF and MgF<sub>2</sub>. Once again our results are in accord with the original findings for NaMgF<sub>3</sub> of Umemoto and Wentzcovitch (2006) who reported a dissociation pressure of ~40 GPa.

Our findings for both NaMgF<sub>3</sub> and KCaF<sub>3</sub>, therefore, support the view expressed previously by Umemoto et al. (2006a), Grocholski et al. (2010) and Tsuchiya and Tsuchiya (2011) that in the natural silicate system as found in the deep interiors of the mantles of large terrestrial exoplanets or in the cores of gas giants, dissociation into high-pressure polymorphs of the simple oxides, MgO and SiO<sub>2</sub>, will occur before the formation of any of the high-pressure structures considered here.

**Acknowledgements** This work was supported by the Natural Environment Research Council (Ref. NE/J009520/1). The authors acknowledge use of the UK supercomputing facilities HECToR and ARCHER and are grateful to the French regional council of Rhône-Alpes for financial support.

**Open Access** This article is distributed under the terms of the Creative Commons Attribution 4.0 International License (<http://creativecommons.org/licenses/by/4.0/>), which permits unrestricted use, distribution, and reproduction in any medium, provided you give appropriate credit to the original author(s) and the source, provide a link to the Creative Commons license, and indicate if changes were made.

## References

- Aguado F, Rodriguez F, Hirai S, Walsh JN, Lennie A, Redfern SAT (2008) High-pressure behaviour of KMF<sub>3</sub> perovskites. *High Press Res* 28:539–544
- Allmann R, Hinek R (2007) The introduction of structure types into the Inorganic crystal structure database ICSD. *Acta Crystallogr A* 63:412–417
- Ammann MW, Brodholt JP, Wookey J, Dobson DP (2010) First-principles constraints on diffusion in lower-mantle minerals and a weak D'' layer. *Nature* 465:462–465
- Angel RJ (2001) EOS-FIT V5.2. Computer program. Crystallography Laboratory, Department of Geological Sciences, Virginia Tech, Blacksburg
- Bernal FL, Yusenko KV, Sottmann J, Drathen C, Guignard J, Løvvik OL, Crichton WA, Margadonna S (2014) Perovskite to post-perovskite transition in NaFeF<sub>3</sub>. *Inorg Chem* 53:12205–12214
- Besançon P, Adolphe C, Flahaut J, Laruelle P (1969) Sur les variétés  $\alpha$  et  $\beta$  des sulfures L<sub>2</sub>S<sub>3</sub> des Terres Rares. *Mat Res Bull* 4:227–238
- Blöchl PE (1994) Projector augmented-wave method. *Phys Rev B* 50:17953–17979
- Boffa Ballaran T, Tronnes RG, Frost DJ (2007) Equations of state of CaIrO<sub>3</sub> perovskite and post-perovskite phases. *Am Mineral* 92:1760–1763
- Crichton WA, Bernal FL, Guignard J, Hanfland M, Margadonna S (2016) Observation of Sb<sub>2</sub>S<sub>3</sub>-type post-post-perovskite in NaFeF<sub>3</sub>. Implications for ABX<sub>3</sub> and A<sub>2</sub>X<sub>3</sub> systems at ultrahigh pressure. *Miner Mag* 80:659–674
- Dobson DP, Hunt SA, Lindsay-Scott A, Wood IG (2011) Towards better analogues for MgSiO<sub>3</sub> post-perovskite: NaCoF<sub>3</sub> and NaNiF<sub>3</sub>, two new recoverable fluoride post-perovskites. *Phys Earth Planet Inter* 189:171–175
- Dobson DP, McCormack R, Hunt SA, Amman MW, Weidner D, Li L, Wang L (2012) The relative strength of perovskite and post-perovskite NaCoF<sub>3</sub>. *Mineral Mag* 76:925–932
- Dobson DP, Miyajima N, Nestola F, Alvaro M, Casati N, Liebske C, Wood IG, Walker AM (2013) Strong inheritance of texture between perovskite and post-perovskite in the D'' layer. *Nat Geosci* 6:575–578
- Dobson DP, Bailey E, Lindsay-Scott A, Brodholt JP, Wood IG, Vocadlo L (2014) Chemical diffusivity of perovskite and post-perovskite from studies of fluoride analogues. Abstract MR41A-4383 presented at 2014 Fall Meeting, AGU, San Francisco, Calif., 15–19 Dec
- Fletcher DA, McMeeking RF, Parkin D (1996) The United Kingdom chemical database service. *J Chem Inf Comput Sci* 36:746–749
- Friedman Z, Melamud M, Makovsky J, Shaked H (1970) Magnetic structure of NaCoF<sub>3</sub>. *Phys Rev B* 2:179–181
- Fujino K, Nishio-Hamane D, Suzuki K, Izumi H, Seto Y, Nagai T (2009) Stability of the perovskite structure and possibility of the transition to the post-perovskite structure in CaSiO<sub>3</sub>, FeSiO<sub>3</sub>, MnSiO<sub>3</sub> and CoSiO<sub>3</sub>. *Phys Earth Planet Inter* 177:147–151
- Geller S (1956) Crystal structure of gadolinium orthoferrite, GdFeO<sub>3</sub>. *J Chem Phys* 24:1236–1239
- Glazer AM (1972) The classification of tilted octahedra in perovskites. *Acta Crystallogr B* 28:3384–3392
- Goldschmidt VM (1926) Die Gesetze der Krystallochemie. *Naturwissenschaften* 14:477–485
- Grocholski B, Shim S-H, Prakapenka VB (2010) Stability of the MgSiO<sub>3</sub> analog NaMgF<sub>3</sub> and its implication for mantle structure in super-earths. *Geophys Res Lett* 37:L14204
- Hohenberg P, Kohn W (1964) Inhomogeneous electron gas. *Phys Rev* 136:864–871
- Hustoft J, Catalli K, Shim S-H, Kubo A, Prakapenka VB, Kunz M (2008) Equation of state of NaMgF<sub>3</sub> postperovskite: implications for the seismic velocity changes in the D'' region. *Geophys Res Lett* 35:L10309
- Knight KS (2009) Parameterization of the crystal structures of centrosymmetric zone-boundary-tilted perovskites: an analysis in terms of symmetry-adapted basis vectors of the cubic aristotype phase. *Can Mineral* 47:381–400
- Knight KS (2011) Centrosymmetric perovskite crystal structures with space group *Pbnm*: crystallographic parameterization of KCaF<sub>3</sub> between 100 and 400 K in terms of the amplitudes of symmetry-adapted basis vectors of the cubic aristotype phase. *Can Mineral* 49:793–808
- Knight KS (2014) A high resolution neutron diffraction study of the crystal structure of neighborite (NaMgF<sub>3</sub>) between 9 K and 440 K. *Am Mineral* 99:824–838
- Knight KS, Darlington CNW, Wood IG (2005) The crystal structure of KCaF<sub>3</sub> at 4.2 and 300 K: a re-evaluation using high-resolution powder neutron diffraction. *Powder Diffr* 20:7–13
- Knight KS, Marshall WG, Hawkins PM (2014) A high-pressure neutron diffraction study of the ferroelastic phase transition in RbCaF<sub>3</sub>. *Phys Chem Minerals* 41:461–472
- Kohn W, Sham LJ (1965) Self-consistent equations including exchange and correlation effects. *Phys Rev* 140:A1133–A1138
- Kresse G, Furthmüller J (1996) Efficiency of ab initio total energy calculations for metals and semiconductors using a plane-wave basis set. *Comput Mater Sci* 6:15–50

- Kresse G, Joubert J (1999) From ultrasoft pseudopotentials to the projector augmented wave method. *Phys Rev B* 59:1758–1775
- Kresse G, Marsman M and Furthmüller J (2010) VASP Guide. Faculty of Physics, Universität Wien, Austria. <http://cms.mpi.univie.ac.at/vasp/vasp/vasp.html>
- Li L, Weidner DJ (2012) Anelasticity and transient creep in  $\text{NaMgF}_3$  perovskite at high pressure. *Phys Earth Planet Inter* 194–195:98–106
- Lindsay-Scott A (2012) The thermoelastic properties of post-perovskite analogue phases. Ph.D. Thesis, University College London
- Lindsay-Scott A, Wood IG, Dobson D, Vočadlo L, Brodholt JP, Crichton W, Hanfland M, Taniguchi T (2010) The isothermal equation of state of  $\text{CaPtO}_3$  post-perovskite to 40 GPa. *Phys Earth Planet Inter* 182:113–118
- Lindsay-Scott A, Wood IG, Dobson DP, Vočadlo L, Brodholt JP, Knight KS, Tucker MG, Taniguchi T (2011) Thermoelastic properties and crystal structure of  $\text{CaPtO}_3$  post-perovskite from 0 to 9 GPa and from 2 to 973 K. *J Appl Crystallogr* 44:999–1016
- Lindsay-Scott A, Dobson DP, Nestola F, Alvaro M, Casati N, Liebske C, Knight KS, Smith RI, Wood IG (2014) Time-of-flight neutron powder diffraction with milligram samples: the crystal structures of  $\text{NaCoF}_3$  and  $\text{NaNiF}_3$  post-perovskites. *J Appl Crystallogr* 47:1939–1947
- Lundegaard LF, Miletich R, Balic Zunic T, Makovicky E (2003) Equation of state and crystal structure of  $\text{Sb}_2\text{S}_3$  between 0 and 10 GPa. *Phys Chem Minerals* 30:463–468
- Martin CD, Crichton WA, Liu HZ, Prakapenka V, Chen JH, Parise JB (2006a) Phase transitions and compressibility of  $\text{NaMgF}_3$  (Neighborite) in perovskite and post-perovskite-related structures. *Geophys Res Lett* 33:L11305
- Martin CD, Crichton WA, Liu H, Prakapenka V, Chen J, Parise JB (2006b) Rietveld structure refinement of perovskite and post-perovskite phases of  $\text{NaMgF}_3$  (Neighborite) at high pressures. *Am Mineral* 91:1703–1706
- Mitchell RH (2002) Perovskites modern and ancient. Almaz Press Inc., Ontario
- Mitchell RH, Alexander M, Cranswick LMD, Swainson IP (2007) A powder neutron diffraction study of the crystal structure of the fluoroperovskite  $\text{NaMgF}_3$  (neighborite) from 300 to 3.6 K. *Phys Chem Miner* 34:705–712
- Monkhorst HJ, Pack JD (1976) Special points for Brillouin-zone integrations. *Phys Rev B* 13:5188–5192
- Mousa AA (2014) First-principles study of structural, electronic and optical properties of the  $\text{KCaX}_3$  ( $X = \text{F}$  and  $\text{Cl}$ ) compounds. *Int J Modern Phys B* 28:1450139
- Murakami M, Hirose K, Kawamura K, Sata N, Ohishi Y (2004) Post-Perovskite phase transition in  $\text{MgSiO}_3$ . *Science* 304:855–858
- O’Keeffe M, Hyde BG (1977) Some structures topologically related to cubic perovskite ( $E2_1$ ),  $\text{ReO}_3$  ( $D0_9$ ) and  $\text{Cu}_3\text{Au}$  ( $L1_2$ ). *Acta Crystallogr B* 33:3802–3813
- Oganov AR, Ono S (2004) Theoretical and experimental evidence for a post-perovskite phase of  $\text{MgSiO}_3$  in Earth’s D’’ layer. *Nature* 430:445–448
- Pauling L (1929) The principles determining the structure of complex ionic crystals. *J Am Chem Soc* 51:1010–1026
- Perdew JP, Burke K, Ernzerhof M (1996) Generalized gradient approximation made simple. *Phys Rev Lett* 77:3865–3868
- Pippard AB (1966) The elements of classical thermodynamics. Cambridge University Press, Cambridge, pp 43–45
- Poirier JP, Peyronneau J, Gesland JY, Brebec G (1983) Viscosity and conductivity of the lower mantle: an experimental study on a  $\text{MgSiO}_3$  perovskite analogue,  $\text{KZnF}_3$ . *Phys Earth Planet Inter* 32:273–287
- Putz H, Brandenburg K (2006) Diamond-crystal and molecular structure visualization. Crystal Impact-GbR, Bonn. <http://www.crystalimpact.com/diamond>
- Rodi F, Babel D (1965) Erdalkaliiridium (IV)-oxide: Kristallstruktur von  $\text{CaIrO}_3$ . *Z Anorg Allg Chem* 336:17–23
- Shannon RD (1976) Revised effective ionic radii and systematic studies of interatomic distances in halides and chalcogenides. *Acta Crystallogr A* 32:751–767
- Shim S-H, Catalli K, Hustoft J, Kubo A, Prakapenka VB, Caldwell WA, Kunz M (2008) Crystal structure and thermoelastic properties of  $(\text{Mg}_{0.91}\text{Fe}_{0.09})\text{SiO}_3$  postperovskite up to 135 GPa and 2,700 K. *Proc Natl Acad Sci USA* 105:7383–7386
- Shirako Y, Kojitani H, Oganov AR, Fujino K, Miura H, Mori D, Inaguma Y, Yamaura K, Akaogi M (2012a) Crystal structure of  $\text{CaRhO}_3$  polymorph: high-pressure intermediate phase between perovskite and post-perovskite. *Am Mineral* 97:159–163
- Shirako Y, Shi YG, Aimi A, Mori D, Kojitani HK, Yamaura KY, Inaguma Y, Akaogi M (2012b) High-pressure stability relations, crystal structures, and physical properties of perovskite and post-perovskite of  $\text{NaNiF}_3$ . *J Solid State Chem* 191:167–174
- Tackley PJ, Amman M, Brodholt JP, Dobson DP, Valencia D (2013) Mantle dynamics in super-earths: post-perovskite rheology and self-regulation of viscosity. *Icarus* 225:50–61
- Tateno S, Hirose K, Ohishi Y (2009) Determination of post-perovskite phase transition boundary up to 4400K and implications for thermal structure in D’’ layer. *Earth Planet Sci Lett* 277:130–136
- Tateno S, Hirose K, Sata N, Ohishi Y (2010) Structural distortion of  $\text{CaSnO}_3$  perovskite under pressure and the quenchable post-perovskite phase as a low-pressure analogue to  $\text{MgSiO}_3$ . *Phys Earth Planet Inter* 181:54–59
- Tschauner O, Ma C, Beckett JR, Prescher C, Prakapenka VB, Rossman GR (2014) Discovery of bridgmanite, the most abundant mineral in Earth, in a shocked meteorite. *Science* 346:1100–1102
- Tsuchiya T, Tsuchiya J (2006) New high-pressure phase relations in  $\text{CaSnO}_3$ . *Am Mineral* 91:1879–1887
- Tsuchiya T, Tsuchiya J (2011) Prediction of a hexagonal  $\text{SiO}_2$  phase affecting stabilities of  $\text{MgSiO}_3$  and  $\text{CaSiO}_3$  at multimegabar pressures. *Proc Natl Acad Sci USA* 108:1252–1255
- Tsuchiya T, Tsuchiya J, Umemoto K, Wentzcovitch RM (2004) Phase transition in  $\text{MgSiO}_3$  perovskite in the earth’s lower mantle. *Earth Planet Sci Lett* 224:241–248
- Umemoto K, Wentzcovitch RM (2006) Potential ultrahigh pressure polymorphs of  $\text{ABX}_3$  compounds. *Phys Rev B* 74:224105
- Umemoto K, Wentzcovitch RM, Allen PB (2006a) Dissociation of  $\text{MgSiO}_3$  in the cores of gas giants and terrestrial exoplanets. *Science* 311:983–986
- Umemoto K, Wentzcovitch RM, Weidner DJ, Parise JB (2006b)  $\text{NaMgF}_3$ : a low-pressure analog of  $\text{MgSiO}_3$ . *Geophys Res Lett* 33:L15304
- Vočadlo L, Price GD, Wood IG (1999) Crystal structure, compressibility and possible phase transitions in  $\epsilon\text{-FeSi}$  studied by first-principles pseudopotential calculations. *Acta Crystallogr B* 55:484–493
- Watson GW, Parker SC, Wall A (1992) Molecular dynamics simulation of fluoride-perovskites. *J Phys: Condens Matter* 4:2097–2108
- Watson GW, Wall A, Parker SC (1995) A molecular dynamics simulation of the effect of high pressure on fast-ion conduction in a  $\text{MgSiO}_3$ -perovskite analogue;  $\text{KCaF}_3$ . *Phys Earth Planet Inter* 89:137–144
- Weir CE, Piermarini GJ (1964) Lattice parameters and lattice energies of high-pressure polymorphs of some alkali halides. *J Res Natl Bur Stand (US)* 68A:105–111
- Wood IG, Knight KS, Price GD, Stuart JA (2002) Thermal expansion and atomic displacement parameters of cubic  $\text{KMgF}_3$  perovskite determined by high-resolution neutron powder diffraction. *J Appl Crystallogr* 35:291–295
- Wood IG, Lord OT, Wann ETH, Thomson AR, Morard G, Mezouard M, Daisenberger D, Jakymiw C, Vočadlo L, Brodholt JP, Lindsay-Scott A, Dobson DP (2017) Beyond post-perovskite:

- high-pressure phase transitions in  $\text{NaCoF}_3$ . To be submitted to Phys Earth Planet Inter
- Wu X, Qin S, Wu Z (2006) First-principles study of structural stabilities, and electronic and optical properties of  $\text{CaF}_2$  under high pressure. Phys Rev B 73:134103
- Xu C, Xu B, Yang Y, Dong H, Oganov AR, Wang S, Duan W, Gu B, Bellaiche L (2015) Prediction of a stable post-post-perovskite structure from first principles. Phys Rev B 91:020101
- Yusa H, Shirako Y, Akaogi M, Kojitani H, Hirao N, Ohishi Y, Kikegawa T (2012) Perovskite-to-postperovskite transitions in  $\text{NaNiF}_3$  and  $\text{NaCoF}_3$  and disproportionation of  $\text{NaCoF}_3$  postperovskite under high pressure and high temperature. Inorg Chem 51:6559–6566